Desalination 355 (2015) 186–196

Contents lists available at ScienceDirect

Desalination

journal homepage: www.elsevier.com/locate/desal

Pilot demonstration of concentrated solar-powered desalination of subsurface agricultural drainage water and other brackish groundwater sources

Matthew D. Stuber [a,*], Christopher Sullivan [b], Spencer A. Kirk [b], Jennifer A. Farrand [b], Philip V. Schillaci [b], Brian D. Fojtasek [b], Aaron H. Mandell [a]

[a] WaterFX, Inc., PO Box 2304, Healdsburg, CA 95448, USA
[b] ATSI, Inc., 415 Commerce Dr, Amherst, NY 14228, USA

HIGHLIGHTS

- A novel renewable-energy powered desalination system is developed and piloted.
- The system integrates an open-cycle heat pump with multi-effect distillation.
- A large parabolic trough solar concentrator is used to power the process system.
- A 49% reduction in thermal energy consumption is demonstrated.
- High scaling propensity agricultural drainage water is desalinated for reuse.

ARTICLE INFO

Article history:
Received 12 June 2014
Received in revised form 17 October 2014
Accepted 24 October 2014
Available online 8 November 2014

Keywords:
Solar desalination
MED
Energy efficiency
Absorption heat pump
Renewable energy

ABSTRACT

The energy–water nexus is addressed with the experimental demonstration of a solar-powered desalination process system. This system was designed for high-recovery treatment of subsurface agricultural drainage water as a reuse strategy as well as other brackish groundwater sources. These water sources may exhibit wide fluctuations in salinity and makeup and pose a high risk for operational troubles due to high scaling potential. A first-of-its-kind open-cycle vapor-absorption heat pump is coupled with a multiple-effect distillation train and a large parabolic trough solar thermal concentrator. Without the heat pump, the distillation operation showed a minimum thermal energy consumption of 261.87 kWh_{th}/m^3. With the heat pump, the thermal energy consumption was reduced by more than 49% to 133.2 kWh_{th}/m^3. This reduction in thermal energy requirement directly translates into a 49% reduction in solar array area required to power a process with the same freshwater production rate as a system without an integrated heat pump. An optimized design was modeled and the thermal energy performance of a commercial system is projected at 34.9 kWh_{th}/m^3 using a 10-effect MED operating at 85% recovery.

1. Introduction

The ongoing worldwide water scarcity problem is compounding with population growth, industrialization and development, economic growth, and climate change. The obvious abundance of saltwater sources on Earth has motivated the development and implementation of desalination technologies, primarily in coastal regions, in an attempt to close the water gap (i.e. the water deficit). Such technologies have been widely adopted in the Middle East and North Africa (MENA) regions, accounting for about 50% of the global installed desalination capacity [1,2]. However, water scarcity is a worldwide problem motivating the adoption of desalination technologies in other regions in recent years. For instance, a report by the International Desalination Association (IDA) [3] projects that the fastest growth in desalination over the next five years is expected to take place in South Africa, Jordan, Libya, Mexico, Chile, India, and China, where their installed capacity is expected to double. Astoundingly, a recent review on the current state and future of desalination states that the current worldwide desalination capacity is growing at a yearly rate of 55% [4].

Water and energy have an inherent interdependence that is typically only explored from an economic perspective (i.e., what is the impact of energy cost on water and vice-versa). However, the interdependency goes deeper than this economic perspective since water consumption is tied to power generation and energy consumption is tied to potable water production. Hussey et al. [5] explored the changing landscape of energy and water of recent years and projections into the future. Interestingly, the authors [5] conclude that as energy sources are diversified

* Corresponding author.
E-mail address: stuber@waterfx.co (M.D. Stuber).

http://dx.doi.org/10.1016/j.desal.2014.10.037
0011-9164/

and modified with emphasis on renewables and carbon capture, there is an increased dependence on water. For example, the worst clean energy source in terms of water usage is dry-rock geothermal which consumes more than five times the water that the standard natural gas combined cycle uses and two-and-a-half times that of a standard coal plant [5]. In this case, energy is harnessed with zero carbon emissions but with a very large water footprint. The UN states that 90% of the global power generation is water intensive [6]. They go on to conclude that "meeting ever-growing energy demands will require seeking coherence between water use and climate change mitigation" [6]. However, producing "new" freshwater sources via desalination brings its own challenges in the form of substantial energy requirements to remove salt from water for all proposed technologies and implementations.

In this paper, an advanced desalination process system, based on multiple-effect distillation (MED), is presented that provides a two-fold improvement in first-law (thermal) efficiency and minimizes the dependence on water-intensive power sources by consuming solar thermal power directly as its primary energy source. A pilot was constructed and operated at the Panoche Drainage District in Firebaugh, CA with the purpose of demonstrating high water recovery and energy efficiency for desalination of subsurface agricultural drainage water for reuse. In the next section, the background on the state-of-the-art will be discussed through a review of the relevant literature as well as motivating this work. Following a literature review, the Materials and methods section will discuss the modeling and simulation methods as well as the pilot system and experimental methods. The results of the simulations and the experiments with the pilot system will be presented along with a thorough discussion and comparison. A projection of the design and performance of a commercial system will then be presented and finally the paper will be concluded.

1.1. Background and motivation

When comparing desalination process systems on a thermodynamic basis, two concepts of efficiency will be referred to: first-law efficiency, which is the typical thermal efficiency of the process, and second-law efficiency, which is typically defined as the ratio of useful work output to the useful work input and quantifies the destruction of thermodynamic availability or exergy.

Desalination technologies are most commonly separated into two categories: thermal methods and membrane methods. As of 2012, the installed capacity of reverse osmosis (RO) membrane technologies was roughly 60% whereas traditional thermal technologies made up roughly 34% [4]. The two common goals in the desalination community spanning the diverse technologies are reducing total specific energy consumption (SC), defined as

$$SC \equiv \frac{\text{energy input (kWh)}}{\text{total water produced } (m^3)}, \quad (1)$$

and reducing the total water production cost.

Despite the widespread adoption of RO, the technology is fairly limited to seawater treatment applications and its dependence on application-specific pretreatment makes the technology relatively inflexible. Global water use is dominated by agricultural operations which account for 70% of consumption [6]. In California, agricultural operations account for roughly 79% of the diverted surface waters and pumped groundwater sources [7]. This has motivated the need for desalination of brackish groundwater for agricultural irrigation as well as desalination of agricultural drainage water for reuse. In [8], low-pressure RO was applied to a low-salinity groundwater feed for production of high-purity water for the beverage industry. The authors noted that despite the more favorable conditions for RO, after about 20 weeks, membrane flux decreased by 10% and the pressure drop increased by nearly 10% due to membrane fouling [8]. Besides the treatment of low-salinity feeds, groundwater and agricultural drainage pose a serious technological and environmental challenge for RO. The environmental challenge comes from high-volume brine waste disposal due to limited recovery. In [9], the environmental challenge was considered with the proposal of zero-liquid discharge (ZLD) for solids recovery. However, technological challenges of the implementation persist. For instance, the highest salinity considered by the authors was 1500–3000 ppm total-dissolved solids (TDS) and in the best case, the system would be operated at 95% recovery producing a brine waste stream with 30,000 ppm TDS [9] or just 3% dissolved solids. In this case, the authors' simulation results predict the SC value of the RO (without ZLD) to be 4.4 kWh_e/m^3.[1] They conclude that, as compared to seawater RO desalination, their approach is more favorable for inland applications [9]. Since the paper was more of an initial feasibility study, the authors did not provide an analysis of scaling and fouling for such source waters at high recovery which is expected to be detrimental to the long-term viability of the proposed solution.

In 2010 McCool et al. [10] investigated the feasibility of RO for treating agricultural drainage in the San Joaquin Valley (the same region as the pilot demonstration in this paper). They considered water sources with salinities ranging within 7000–23,000 ppm TDS with wide relative yearly variations. They show that with proper scaling mitigation techniques, the recovery limits are between 44% and 68% across the region [10]. However, they conclude that any implementation of RO for treating these water sources would require site-specific process optimization as well as real-time monitoring for fouling mitigation as a result of feed chemistry variations [10]. Such a monitoring device was constructed and tested using agricultural drainage water at the Panoche Water District in the San Joaquin Valley by Thompson et al. [11] for rapid field evaluation and optimization. The study verified the effectiveness of such a monitoring device and validated the expectations of rapid scaling causing dramatic performance decline at 65% recovery from a 14,400 ppm TDS source [11]. Despite these advancements, due to the high scaling propensity of brackish groundwater and subsurface agricultural drainage water sources, pretreatment costs are high and recovery is limited for RO technologies and therefore cannot adequately address the environmental issue of brine waste disposal.

Of the major advancements in energy reductions, RO stands out partly due to its currently being the dominant technology worldwide but also because the improvements have been quite extreme in the last 40 years. In [12] the authors present a very striking chart that shows the energy consumption of RO decreasing to about 12% of its value in 1970. This reduction primarily represents major advancements in membrane technology over the years. However, the authors state that conveyance and pretreatment still require a relatively high amount of energy input (>50% of the membrane requirement), representing limitations in the technology even if the membranes are operating at their theoretical maximum efficiency [12]. Cohen-Tanugi et al. [13] further explored this idea and concluded that minimal improvement in overall water cost can be realized even if membrane permeability was to increase three-fold. Furthermore, despite reductions in the SC value, the high-pressure pumps required for RO are still electrically driven. Therefore, they require substantial amounts of electrical power at-scale which poses new challenges when considering the energy–water nexus, such as requiring a high thermodynamic availability energy source, as well as the technological and environmental limitations for the application to brackish groundwater and agricultural drainage water.

The two popular thermal desalination technologies are multi-stage flash (MSF) and MED, also referred to as multi-effect evaporation (MEE). Due to its early adoption in desalination, MSF still has the highest installed capacity of all thermal methods [4,14,15]. However, MED has the competitive advantage over MSF as it offers greater efficiency and reduced water cost due to lower capital costs as well as operating and maintenance costs [14,16–18]. Furthermore, for the same overall performance, MED requires substantially less electrical energy

[1] The subscript 'e' denotes electrical energy and 'th' will denote thermal energy.

for pumps by a factor of about 30% (just about 1 kWh_e/m^3 for an 11-effect MED) [16–18]. Despite consuming much more energy overall than RO, MSF and MED technologies are almost entirely powered by low-quality thermal energy directly (except for some electrical pumps). Furthermore, as stated in [15], "due to their reliability and massive field experience" thermal methods are able to keep their water costs competitive with RO. In [19], the authors present a thermo-economic analysis of MSF and MED. They conclude that from an economic perspective, a hybrid MED–MSF system will yield a total product water cost that is 9% lower than the MED system on its own [19]. Similarly, in [20], the structural optimization of a seawater desalination superstructure system model yielded an optimal design that combined both MED and MSF stages.

In [21], Mistry and coworkers formally defined the second-law efficiency specifically for desalination processes. They demonstrated that the single largest source of entropy generation in an MED system (specifically a 6-effect feed-forward system) was in the final condenser where the final effect distillate vapor is condensed. By reducing the size of the condenser or eliminating it altogether may dramatically increase the second-law efficiency of MED [21]. In order to achieve this and optimize efficiency and water cost of thermal systems, there has been active research in coupling them with low-cost heat recovery devices. These heat recovery devices reduce the size of the final condenser and capture the latent heat of the low-quality final effect (or a fraction of some intermediate effect) distillate vapor and increase its temperature and pressure to be reused as driving steam for the first effect. There are four main heat recovery devices available for this task: mechanical vapor compression (MVC), thermal vapor compression (TVC), adsorption heat pumps (ADHP), and absorption heat pumps (AHP). MVC and TVC are the most commonly implemented heat recovery devices. MVC uses mechanical work to drive a compressor to compress low temperature/pressure steam to higher temperatures and pressures. The application of MVC is quite limited to smaller capacities and, barring some examples of MED-coupled units, mostly applied with only a single-effect distillation unit. Furthermore, due to compressors being predominantly driven by electric motors, they pose the same challenges as pumping for RO in terms of the energy–water nexus [22]. TVC uses a steam-jet ejector or nozzle which consumes high pressure motive steam to increase the pressure and temperature of a low-pressure steam source by using the Venturi effect. Due to the simplicity of TVC and the higher thermal efficiency of MED, TVC is most commonly combined with MED. The recent works of Dahdah and Mitsos [23] on the structural optimization of seawater desalination system superstructure models yielded two new optimal designs that combined TVC, MED, and MSF. Despite the simplicity of TVC and the widespread adoption for increasing the efficiency of MED (and MSF), TVCs have a low second-law efficiency [21,24] and so are rather limited in the heat recovery performance they can offer. TVCs are also inflexible at operating at partial capacity and any deviation in operations away from their design point rapidly decreases their efficiency [25].

The final two vapor compression technologies for minimizing the requirement of the final condenser are ADHP and AHP. Both ADHP and AHP implementations for desalination applications are quite similar. As the names suggest, ADHPs utilize special hygroscopic solid media to adsorb low-pressure steam, releasing its latent heat, whereas AHPs utilize special hygroscopic liquid media to do the same. For more on the fundamentals of ADHPs and AHPs, the reader is directed to [26] and [27], respectively.

The work on ADHP–MED combined systems is limited to a few applications with renewable energy powered applications [28–31]. In each case the system performance is quite low and the applicability is limited. Although ADHP emerging technologies are well-suited for waste-heat and some renewable energy applications, poor performance and operational challenges of coupling batch and continuous processes make their current application to commercial desalination infeasible.

The most competitive heat-recovery device is the AHP. Aly [32] proposed using an AHP for multi-effect distillation to be powered by waste heat from the exhaust of a gas turbine. They simulate that with a 14-effect MED system, the combined process could produce 44% more water for the same energy input as other competing waste-heat recovery technologies of the time [32]. Fathalah and Aly [33] showed that combining an AHP with MED would provide a major performance boost over MED on its own. Furthermore, they identified that although AHPs may have worse overall efficiency than MVC heat pumps, the thermal-powered nature of AHPs allows for natural coupling with solar thermal receivers [33]. Right around the same time, researchers constructed a demonstration AHP–MED combined system for seawater desalination [25,34]. A second prototype was constructed about 10 years following the first and experiments yielded promising results demonstrating an extremely low SC of 32 kWh_{th}/m^3 [25,34]. A numerical comparison of an open-cycle AHP coupled with a single distillation stage was given by Mandani et al. [35]. They showed that the theoretical system performed 50–70% higher than comparable TVC–MED systems [35]. Despite being thoroughly-studied and well-known technology, the adoption and implementation with desalination applications are extremely limited. Interestingly, as of 2010, only two pilot facilities of combined AHP–MED systems have been constructed worldwide [34] and each employed closed-cycle AHPs.

The robustness and flexibility of MED for treating high scaling propensity water, especially those from sources with fluctuating quality such as subsurface agricultural drainage, make the technology an ideal candidate for treating subsurface agricultural drainage water and other brackish groundwater sources. Furthermore, since it is a thermal-driven technology that operates at relatively low temperatures (typically <70 °C), it is an ideal candidate for solar-thermal power when operating in regions with adequate solar performance. For this reason, MED was selected to be the technology to be deployed for pilot demonstration at the Panoche Drainage District. Furthermore, due to the high performance, operational flexibility, and the fact that they are also thermal-driven processes, the AHP was selected to be the vapor-compression technology of choice for maximizing the first- and second-law efficiency of the MED. Although AHPs are operated at a higher temperature than the MED—and therefore require higher thermodynamic availability energy sources than MED alone—they offer a favorable mating of medium-temperature concentrated solar power and low-temperature MED from a second-law perspective. Similarly, the increased simplicity, increased performance, and reduced capital investment of an open-cycle AHP design make it an ideal candidate in a first-of-its-kind fully-combined solar-powered AHP–MED desalination process system.

2. Materials and methods

The high-level objective in designing the desalination process system was to maximize first- and second-law efficiencies which directly minimizes losses, specific energy consumption, and reduces the capital cost associated with the concentrated solar thermal power system. In [25], Alarcón-Padilla and coworkers explained that one of the most important benefits of dramatically improving the specific energy consumption of traditional MED when considering solar power is the significant reduction in the size of the solar array; translating into significant reductions in capital costs as well as operating costs.

2.1. Process modeling and simulation

The modeling and steady-state simulation of the desalination process were performed using the OpenModelica language [36] for equation-oriented simulation. The empirical models of the thermophysical properties of saltwater were taken from [37]. The absorption fluid considered was an alkaline nitrate solution referred to as Alkitrate. Alkitrate was originally studied in [38–40] and an improved mixture ratio and vapor–liquid equilibrium correlations were given in [41]. The thermodynamic

properties of water were taken from the steam tables. For this study, the performance of the thermal power block, consisting of the concentrated solar-thermal receiver array and backup heater, was not modeled since it was assumed that the heat supplied to the process was constant (see Assumption 2.1-5).

Since the modeling and simulation of AHP–MED systems have been extensively studied, as discussed in the previous section, the intention of modeling and simulation here is not to explore the fundamental behavior of AHP–MED systems but to predict the performance of a real system and use data collected to validate the models. Such information may then be used to further explore and understand any anomalous experimental data or to verify modeling assumptions. This information is especially useful for minimizing uncertainty in designing and optimizing a large-scale commercial system. Unless noted otherwise, the modeling assumptions used herein are formalized in Assumption 2.1.

Assumption 2.1. Modeling assumptions

1. No heat losses to the environment
2. Constant temperature difference between the condensing steam and the boiling saltwater in each distillation effect
3. Each vessel is well-mixed
4. Thermophysical properties of seawater apply to brackish groundwater
5. Constant heat supply to the process at constant conditions
6. Product water density is constant at 1000 kg/m^3.

Assumption 2.1-6 may seem a bit strange since the density of water at a given temperature and pressure is well-known. However, since the conditions of the product water leaving the plant may vary depending on the operating conditions of the plant, a constant conversion (between mass and volume) is needed in order to make a fair comparison across all sets of data. This is only required because oftentimes the capacity of a desalination plant is given in [volume] / [time] units.

2.2. Pilot system

Fig. 1 shows the process flow diagram of the solar-AHP–MED pilot system (omitting the backup heater). A heat transfer fluid is pumped through the solar array, absorbing solar radiation, in a closed-loop configuration maintaining a set temperature. The fluid delivers the solar heat to the steam generator (also referred to as the generator or desorber) of the AHP. The AHP is an open-loop system consisting primarily of an absorber and a generator. The MED section acts as the condenser, expansion valve, and evaporator/chiller of a traditional closed-loop AHP, depicted in Fig. 2.

The flow rate of the heat transfer fluid sent to the AHP is manipulated to maintain a set point for the produced steam pressure leaving the generator. For example, if steam pressure drops, the controller will increase the heat input to the process and vice-versa. The reader should note that the solution pump, the solution expansion valve, and the economizer heat exchanger depicted in Fig. 2 are intentionally omitted from Fig. 1 for clarity.

The steam produced in the generator condenses in the first effect and its latent heat is captured by the saltwater, causing it to boil and produce steam. The boiling saltwater becomes increasingly more concentrated as steam is produced. The boiling saltwater is recirculated to increase the overall heat transfer coefficient and minimize scaling. A fraction of the recycled saltwater is sent forward to the second effect (i.e., feed-forward). The distillate steam produced in the first effect is condensed in the second effect and its latent heat is captured by the saltwater, causing it to remain boiling and producing steam. This process continues in the third effect in the same manner. The steam condensed in the first, second, and third effects is extracted as freshwater product. The distillate steam produced in the third effect is sent to the absorber. A final condenser is implemented to help control the overall mass balance of steam, if necessary depending on the operating conditions. The flow of the condenser cooling water is automatically manipulated to control the steam pressure in the final effect and the absorber to ensure that the mass of steam sent back to the heat pump is the same as what is sent to

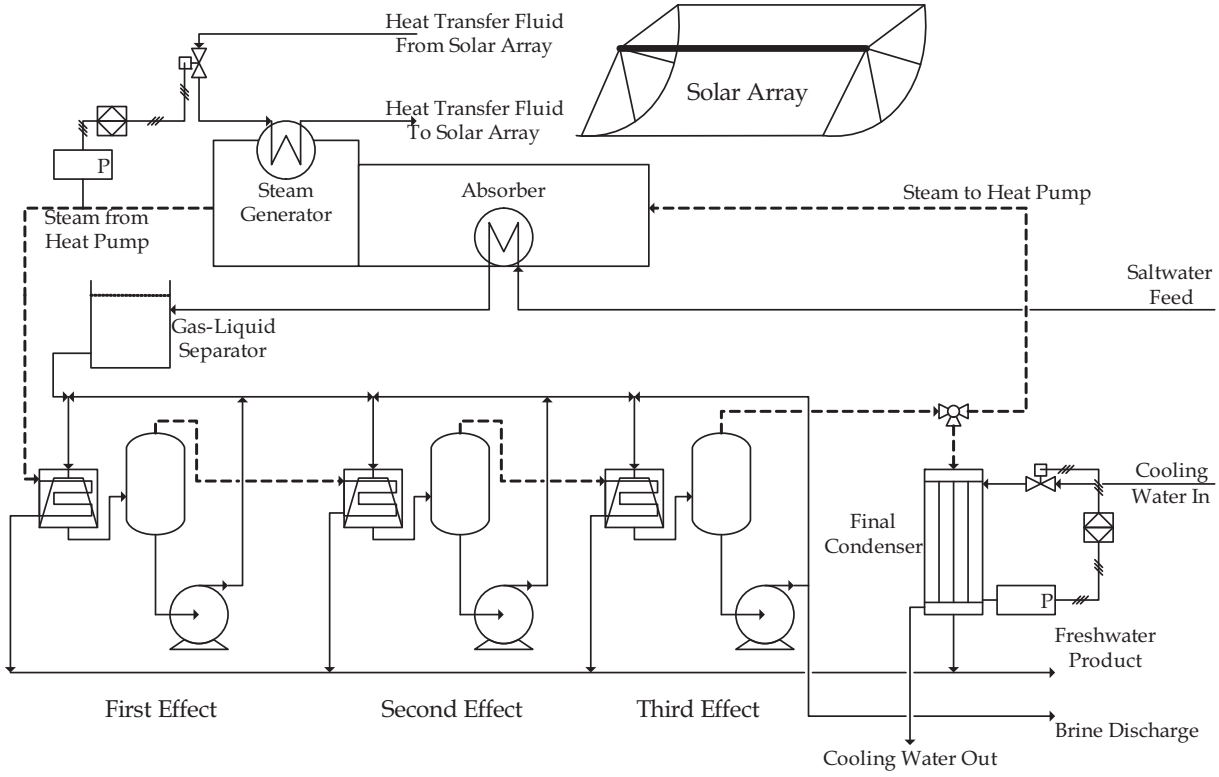

Fig. 1. The process flow diagram for the solar-powered open-loop AHP combined with an MED.

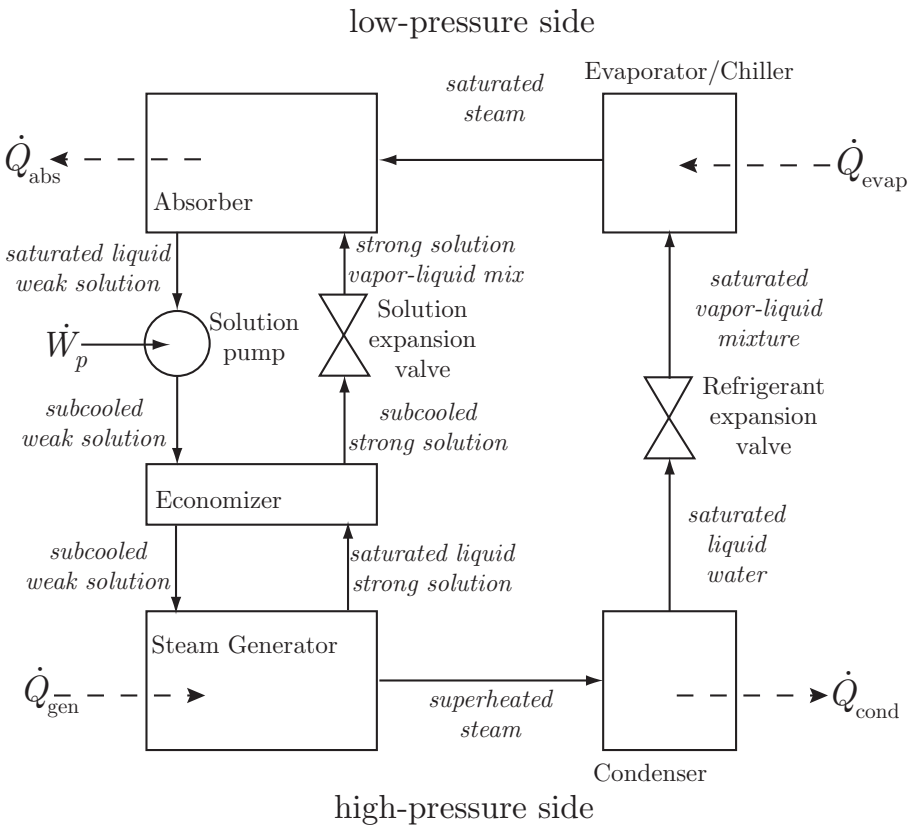

Fig. 2. The process flow diagram of a simple single-effect closed-loop absorption heat pump.

the first effect. Similarly, there is a recirculation valve that redirects the first-effect steam condensate back to the absorber to ensure the mass balance of water in the event that distillate steam production from the third effect is limited (e.g., during startup or a process upset).

Saltwater is fed to the absorber as cooling water where it is heated by the exothermic absorption phenomenon taking place within. The heated saltwater is taken as preheated feed and is then sent to a gas–liquid separator where any non-condensible gases are separated before being fed to the first effect of the MED, which operates under vacuum conditions.

The solar array used to power the process is shown in Fig. 3. The array is a large parabolic trough solar thermal concentrator supplied by SkyFuel, Inc. (Arvada, CO). It has an aperture area of 656 m^2 and a claimed peak thermal efficiency of 73.7% based on 1000 W/m^2 solar irradiance. The heat transfer fluid used to carry heat from the array to the process is Therminol XP (Eastman Chemical Company, Kingsport, TN) which is a food-grade mineral oil for minimizing any hazard for human or wildlife exposure and minimal environmental impact in the case of a spill. A backup heater (CEI Enterprises, Albuquerque, NM) fired by propane was also integrated into the solar oil loop in order to

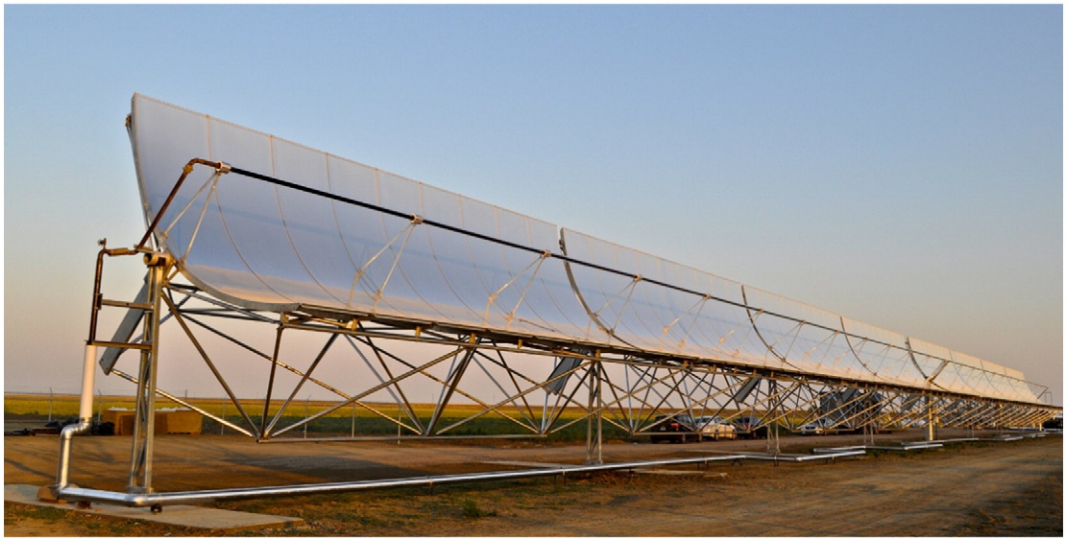

Fig. 3. The large parabolic trough solar thermal concentrator used to power the AHP–MED desalination process.

carry out experiments when solar conditions did not permit operation with the array.

The MED system (Fig. 4) is a re-purposed 3-effect plate-and-frame forced-circulation distillation train originally supplied by APV (SPX, Charlotte, NC) and refurbished for this project. Each effect consists of the rising/falling plate-and-frame evaporator/condenser heat exchanger and a horizontal cylinder disengaging chamber for separating the steam from the boiling saltwater. The MED is configured with each distillation effect having its own recirculation pump and a manual valve for controlling the recycle ratio for high-recovery experiments. A liquid-seal vacuum pump is required to evacuate the MED system during startup and to extract non-condensable gases that may build up during operation due to small vacuum leaks or gas entrainment in the feed. For the experiments conducted herein, there were no feed preheat heat exchangers for reducing the temperature of the condensate streams before they leave the control volume (i.e., hot freshwater leaves the process as the product). The only pretreatment used was microfiltration with a Pentek 100 μm polyester felt filter bag (Pentair, Milwaukee, WI) for removal of suspended solids and an injection of Belclene 200 antiscalant (BWA, Tucker, GA) at 2 ppm. In order to realize capital cost savings, the pilot system was constructed with minimal automatic control and no data-logging capabilities. All data must be recorded by hand predominantly read from analog gauges.

The AHP is a custom-designed single-effect unit constructed by Energy Concepts (Annapolis, MD). It has a peak cooling capacity of 90 tons of refrigeration (316.5 kW) and a COP for heating of 2.0; therefore capable of delivering about 600 kW of heat for the desalination section. For this paper, the absorbent used was the Alkitrate (53 $LiNO_3$: 35 KNO_3: 12 $NaNO_3$) alkaline nitrate mixture. A portion of the heat that evolves in the absorber due to the exothermic absorption of steam is captured by preheating the incoming saltwater feed.

The pilot system was operated in two distinct modes. First, the system was operated in "MED-only mode" without the heat pump for heat integration. The second mode is the "AHP–MED mode," which, as the name implies, is the fully-integrated AHP–MED system depicted in Fig. 1. For both modes of operation the agricultural drainage water feed was taken from the tile sump TS-3 at the Panoche Drainage District which contains a mixture of water drained from the surrounding 90,000 acres of agricultural operations. The salinity of the feed varied throughout operations but the break-down of the primary constituents is shown in Table 1. The representative analysis, from which the data in Table 1 was obtained, showed nearly a one-to-one correspondence between conductivity (in μS/cm) and TDS (in ppm). For the purposes of simulation, it will be assumed that the same proportionality applies.

2.2.1. MED-only operations

In MED-only mode, the heat from the solar-thermal receiver was consumed by a closed-loop boiler system raising driving steam at 30 kPa (69.1 °C) to power the MED system. The feed was not preheated and the distillate steam produced in the third effect was condensed in a final condenser, rejecting its latent heat to cooling water discharged to the environment. This mode is clearly the least efficient since there is no heat recovery at all. However, the objective was to characterize the baseline performance of the MED system. Multiple experiments were conducted with varying water recovery.

Table 1
The break-down of the predominant ions found in the drainage water treated from TS-3 based on a representative sample with 16,300 ppm TDS as verified by an independent laboratory.

Ion	Mass % of TDS	Method
Bicarbonate	1.942	SM2320B
Boron	0.332	EPA200.7/11.2
Calcium	3.336	EPA200.7/11.2
Chloride	22.595	EPA300.0
Magnesium	2.542	EPA200.7/11.2
Nitrate	1.100	EPA300.0
Potassium	0.032	EPA200.7/11.2
Selenium	0.002	EPA200.8
Silica	0.215	SM4500-Si D
Sodium	28.244	EPA200.7/11.2
Sulfate	39.659	EPA300.0
Trace minerals	0.001	EPA200.7/11.2
Total	100.00	

2.2.2. AHP–MED operations

The heat transfer fluid was delivered to the AHP from the solar array at a set point of 180 °C. Steam generated in the AHP was delivered to the first distillation effect at 30 kPa with varying degrees of superheat depending on the operating conditions of the heat pump. The concentrations of the absorbent solution in the generator (strong solution) and the absorber (weak solution) vary throughout operations and are predominantly self-regulating with some influence from the operator. The final condenser was kept in place, as discussed in the process description above, and the flow of cooling water was automatically manipulated to control the steam pressure in the final effect and the absorber. Multiple experiments were conducted with varying water recovery.

3. Results and discussion

3.1. MED-only operations

The MED-only experiments were conducted over a period of 6 days with a total of about 30 h of operations. The data recorded for each day were averaged and the performance of the plant was compared to the expected values given by simulation. A summary of the experimental

Fig. 4. Two views of the 3-effect plate-and-frame MED system used for the pilot demonstration before insulation was applied.

Table 2
The experimental results recorded during the MED-only operating phase. Note that these data are the time-averaged steady-state results for each day.

MED-only experimental results						
Day	1	2	3	4	5	6
<$\dot{Q}_{in}$> [kW]	121.6	134.4	114.1	73.51	83.43	96.37
<Prod. flow> [gpm]	1.528	2.083	1.934	1.058	1.101	1.489
<PR>	1.887	2.484	2.522	2.376	2.250	2.262
<SC> [kWh_{th}/m^3]	399.91	261.87	268.24	311.43	313.91	297.84
<Feed Cond.> [μS/cm]	21,800	23,000	24,300	23,390	26,300	23,170
<Recovery>	27%	30%	54%	41%	31%	60%
<Feed temp> [°C]	25.5	27	27	27	27	27
<ΔT_1> [°C]	7	9	9	9	9	8

data averaged over each day is given in Table 2. Here, the instantaneous performance ratio (PR) is defined as

$$PR \equiv \frac{\dot{m}_{prod}\Delta\hat{H}_v^{ref}}{\dot{Q}_{in}} \tag{2}$$

where $\dot{m}_{prod}$ is the total mass flow rate of product water in kg/s, $\Delta\hat{H}_v^{ref}$ is the latent heat of vaporization of water, in kJ/kg, at a reference temperature taken to be $T_{ref} = 73$ °C, and $\dot{Q}_{in}$ is the heat input to the process in kW. The PR value represents the mass of freshwater product that can be produced per mass of steam (at 73 °C) fed to the process. It is a metric for comparing the first-law efficiencies of thermal processes. The reader should note that the choice of the reference temperature is to maintain a standardized definition for PR for valid performance comparisons within the community.

It can be seen from the results in Table 2 that the performance of the system, in terms of SC and PR, increases with the percent recovery. This is relatively intuitive because at low recovery, a larger percentage of the total heat input is leaving with the concentrated brine discharge and therefore contributes less to freshwater production. Alternatively, at high recovery, a larger percentage of the total heat input is captured for freshwater production.

The MED system was modeled prior to construction of the pilot system to aid in the initial design and optimization. The inputs to the model were taken to be the solar heat input ($\dot{Q}_{in}$), the conductivity of the saltwater feed, the recovery, the temperature of the saltwater feed, and temperature difference between the condensing steam and the boiling temperature of the saltwater between each distillation stage (ΔT_1). Simulations at the conditions observed in Table 2 were performed and the results are found in Table 3 in terms of the percent deviation of the experimental data from the model:

$$\%\ \text{deviation} = \frac{(y_{measured} - y_{model})}{y_{model}} \cdot 100\%. \tag{3}$$

Parametric plots of the pilot data and the simulation data for the PR and SC values are shown in Fig. 5 as functions of the percent recovery. As previously mentioned, the system is expected to be more efficient, from a first-law perspective, as the recovery increases. From the results summarized in Table 3, the model is in good agreement with the actual pilot system. For MED-only operations, it was observed that Assumption 2.1-2 may not be valid. The data shows that the temperature difference in the first distillation effect is oftentimes two to three times more than that of the subsequent effects. This is likely due to the fact that the saltwater feed is not preheated in this mode and since the driving steam is not superheated, a portion of the latent heat goes towards heating the saltwater from the feed temperature up to saturation. Similarly, without preheating the saltwater before it is fed to the first effect, it carries with it a considerable amount of dissolved non-condensable gases. When the saltwater is heated in the first effect, gases come out of solution and effectively raise the operating pressure of the first effect. In order to maintain steam production, these gases must be continuously removed by the vacuum pump. Operating with the first effect partially open to the vacuum source reduces the operating pressure of the effect and therefore the vapor pressure of water in the effect, increasing the temperature difference.

Table 3
The relative deviation (%) of the experimental data from the model for MED-only operations.

MED-only model vs. data						
Day	1	2	3	4	5	6
Prod. flow	−1.2425	10.839	5.8581	−3.4953	−6.5838	−4.2316
PR	1.0777	21.031	7.3844	8.5713	8.479	−4.4519
SC	15.540	−16.831	−2.4577	5.4649	0.7616	9.1353

3.2. AHP–MED operations

The fully-combined solar-AHP–MED experiments were conducted over a period of about 50 days with nearly 400 h of up-time. The data pertaining to each experimental run were averaged and the performance of the plant was compared to the expected values given by the simulation. Fig. 6 shows the PR values and SC values as functions of the percent recovery and the saltwater feed preheat temperature (T_f). The numerical data can be found in Table 4.

The characterization of the performance of the system is more complicated than the MED-only configuration. This is because the performance is sensitive to two competing influences that are linked to one another: feed rate and recovery. Since the saltwater is being preheated in the absorber, its flow rate must be sufficient to capture the heat that evolves from the exothermic reaction. The flow rate of the saltwater feed can be controlled by manipulating the final preheat temperature, T_f (i.e., the temperature of the saltwater being fed to the first effect); however, T_f has an upper bound which is the steady-state temperature of the absorber. Alternatively, if T_f is set too low, then a large feed rate is required. Since the feed rate is constrained by the capacity of the MED system and the heat input, if T_f is set too low, then some portion of the saltwater feed would need to be discharged to the environment, reducing the PR value and increasing the SC value. If the system was to be operated at high recovery, then the performance of the MED section would increase (i.e., higher PR value and lower SC value) according to the results previously discussed. However, due to the aforementioned limited capacity of the system, more heat will be rejected to the environment in the form of discharging a portion of the preheated saltwater. In other words, the MED is more efficient at high recovery but more heat is captured by the heat pump when operating at low recovery (for the same heat input). The simulation results in Fig. 6 demonstrate this result clearly.

The experimental results for the AHP–MED operations appear to exhibit the expected behavior, predicted by the simulation, for the higher feed temperatures ($T_f \geq 65$ °C). However, for $T_f < 65$ °C the performance of the system seems to increase with recovery. The system seems to follow the behavior of the model until the data points for recovery greater

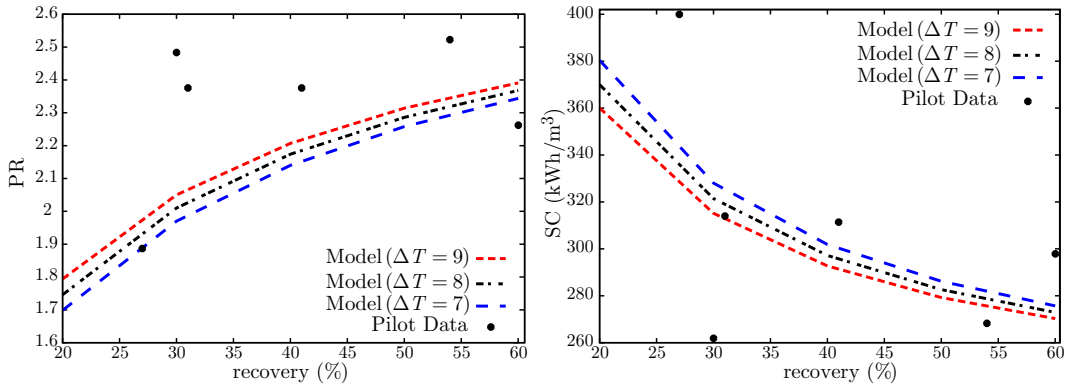

Fig. 5. The parametric plots of the PR values (left) and the SC values (right) as functions of the recovery and temperature difference between effects for the measured pilot data and the model data.

than 59%. This is most likely due to the inability of the simplified heat pump model to capture the internal behavior of the actual heat pump implemented in the pilot plant. Due to the limited published information on the thermophysical properties of Alkitrate, the accuracy of the heat pump model may be inadequate under certain operating conditions. As a whole, the data also appears to be fairly noisy, which contributes to the perceived departure from the simulation results. This is primarily due to the fact that the data was recorded manually from analog gauges, as mentioned in the process description above. The shear volume of data coupled with the time delay inherent to manual recording compounds this noise.

From Table 4, the best observed PR value was 5.269 and the best SC value was 133.2 kWh_{th}/m^3. The best observed PR value from the MED-only operations was 2.522 and the best SC value was 261.87 kWh_{th}/m^3. The AHP–MED values represent a 108.9% increase in the PR value and a 49.1% reduction in the heat input over the MED-only values. This corresponds with a peak COP of heating of between 1.966 and 2.089. From the simulation, the MED has a peak PR value of about 2.5 and a peak SC value of about 259 kWh_{th}/m^3. From the simulation, the AHP–MED has a peak PR value of about 4.61 (at $T_f = 75$ °C and 20% recovery) and a peak SC value of about 140 kWh_{th}/m^3. This represents about an 84% increase in PR value and a 46% reduction in SC over the MED-only system. Therefore, the peak observed performance of the pilot system was observed to be about 5%–13% better than the model.

3.3. Scaling on the MED heat transfer surfaces

As mentioned in Section 1, the MED technology was chosen due to its robustness and flexibility for treating high scaling propensity water sources. As part of the characterization of the performance of the solar-AHP–MED pilot system, the heat transfer properties of the first distillation effect were closely monitored. Monitoring the heat transfer performance allowed for the characterization of the impact of scaling on the heat transfer surfaces. The salts expected to be primarily responsible for adversely affecting performance, especially when treating agricultural drainage water, are $CaCO_3$, Na_2SO_4, and $CaSO_4$. This is because solid precipitation of each of these compounds occurs under heating. The first effect was considered to be the most susceptible to performance degrading scaling for two reasons. First, under normal operations, it is the highest temperature effect in the train. Second, although the saturation temperature of the steam delivered from the AHP is about 69 °C, the steam may exhibit up to 25 °C of superheat. This high temperature may cause local hot spots that cause rapid precipitation of the scaling compounds.

Following about 20 days of operation, the MED plates were opened and manually cleaned. Following this cleaning step, about 30 days of operations and experiments were carried out measuring the heat transfer characteristics of the first effect. In Table 4, the final column labeled ΔT_1 shows the observed steam saturation temperature difference in the first

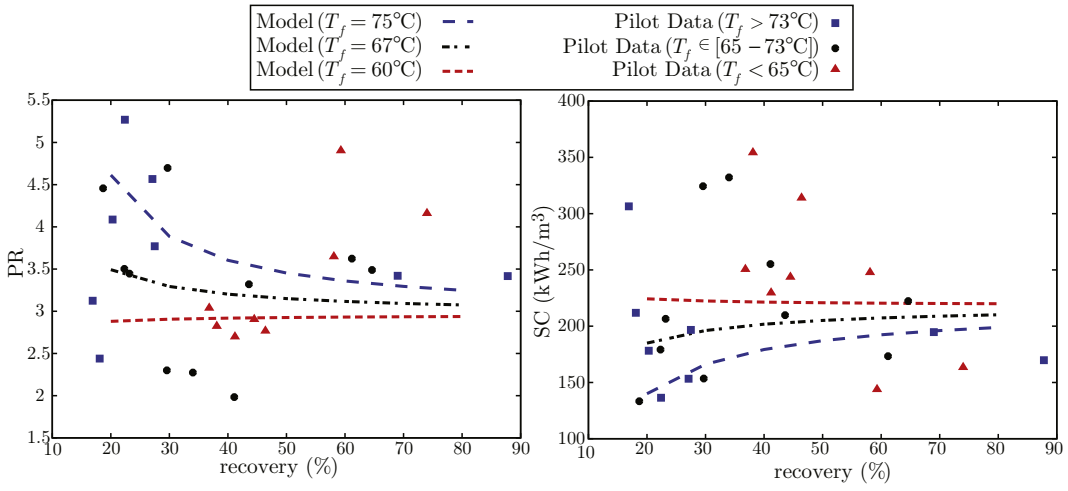

Fig. 6. The parametric plots of the PR values (left) and the SC values (right) as functions of the recovery and the feed preheat temperature for the measured pilot data and the model data.

Table 4
The experimental results obtained from the AHP–MED operations.

AHP–MED experimental results							
$<\dot{Q}_{in}>$ [kW]	<Prod. flow> [gpm]	<PR>	<SC> [kWh_{th}/m^3]	<Feed Cond.> [μS/cm]	<Recov.> [%]	$<T_f>$ [°C]	$<\Delta T_1>$ [°C]
114.4	1.97	2.699	229.7	22,800	41.2	60.0	3
120.5	2.86	3.770	196.7	24,900	27.5	75.0	5
117.0	1.61	2.439	211.9	25,100	18.1	75.0	5
100.0	3.09	4.567	153.3	25,800	27.1	75.0	2
108.3	1.40	1.982	255.2	25,500	41.1	70.0	2
84.7	1.68	3.039	250.6	25,500	36.8	60.0	2.5
119.4	1.57	2.301	324.3	22,500	29.6	68.0	2
82.8	2.14	3.417	169.8	1000	87.8	75.0	3
115.6	2.70	3.488	222.3	25,800	64.6	72.0	3
98.8	2.09	3.125	306.5	20,600	16.9	76.0	2
118.0	3.10	3.319	209.8	20,900	43.6	73.0	2
94.4	3.05	5.269	136.4	21,000	22.4	75.0	2.5
113.7	3.06	4.087	178.2	20,500	20.3	74.0	2.5
112.6	3.53	4.698	153.4	20,400	29.7	73.0	3.5
114.7	2.63	3.504	179.1	19,000	22.3	71.0	2.5
55.8	1.92	4.458	133.2	19,700	18.7	73.0	2
105.0	2.40	3.445	206.5	19,600	23.2	72.0	2.5
117.2	2.75	3.420	194.7	700	69.0	76.5	2.5
91.8	1.37	2.272	332.1	1000	34.0	65.0	2.5
107.7	1.99	2.768	314.0	1200	46.4	60.0	4.5
139.2	3.35	3.648	247.8	1100	58.1	54.0	5.5
125.2	3.71	4.904	143.9	800	59.3	63.5	5.5
124.6	3.36	3.625	173.4	25,900	61.2	66.6	6.5
137.7	3.70	4.161	163.5	31,700	74.0	63.0	5
133.4	2.53	2.905	243.7	32,200	44.5	53.9	3.5
133.2	2.37	2.824	354.3	34,500	38.1	51.2	2.5

effect (between the driving steam from the AHP and the produced steam from the saltwater) for each experiment. Fig. 7 shows the overall heat-transfer coefficient (U) of the first effect for nearly 30 days of operation following the initial cleaning. It can be seen that prior to in-situ cleaning (marked in Fig. 7), U exhibits an overall decreasing behavior likely due to scale build-up. The first eleven days of data show a peak value of over 2300 W/m^2-K and an average value of roughly 1600 W/m^2-K. The manufacturer's established range is 500–2500 W/m^2-K so this is likely to correspond with the optimal performance. The lowest value observed was about 700 W/m^2-K prior to in-situ cleaning. The average value prior to in-situ cleaning was about 1300 W/m^2-K. The plates were opened at this point and the heat transfer surfaces inspected prior to in-situ cleaning. It was confirmed that measurable scale formation was present. Without cleaning, the plates were reassembled and the in-situ cleaning was performed. In-situ cleaning consisted of opening each disengaging chamber and adding a dose of HCl. Each distillation effect was placed in full-recycle mode circulating the acid wash for about 45 min. Finally, the solution was neutralized and the saltwater was drained from each effect. From Fig. 7 the effects of cleaning can be seen. Following cleaning, U increased by approximately 54% and exhibits a generally increasing trend over the next few days. The corresponding affine regressions are also plotted in Fig. 7 demonstrating these trends. For comparison, the average U value following cleaning was about 1270 W/m^2-K.

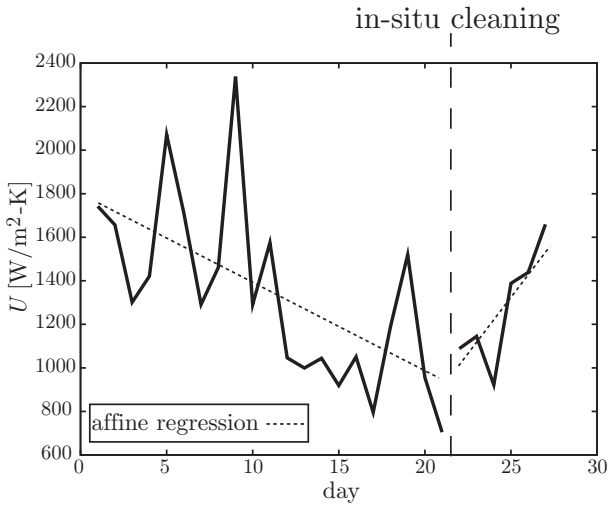

Fig. 7. The observed overall heat transfer coefficient (U) in W/m^2-K of the first distillation effect.

What is perhaps most important when discussing scaling is that no correlation between the system's overall (first-law) efficiency and scaling can be determined from the collected data. That is, even in the face of scaling, the performance of the system in terms of PR and SC remains unaffected. Furthermore, because of this, for a given heat input the freshwater production rate remains unaffected. It should be noted that this may not always be the case, especially when operating with many more distillation effects in the MED train. For instance, if substantial scaling is apparent, then for a given heat input a greater ΔT across the scaled heat transfer surfaces will be required, reducing the second-law efficiency of the MED system. Furthermore, if ΔT gets too large, then the overall temperature difference between the driving steam (from the generator) and the distillate steam from the final effect (i.e., the temperature lift) will increase and the COP of heating for the AHP will decrease according to the second-law of thermodynamics. If the COP decreases, then the PR value will decrease and the SC value will increase. To mitigate the effects of scaling, regularly scheduled in-situ cleaning is recommended when treating agricultural drainage water or other high scaling propensity water sources. Furthermore, to prevent hot spots and maintain uniform heating of the saltwater, it is important that the brine-side of the heat transfer surfaces remain fully-wetted. For this reason, it is imperative that the liquid holdup in each disengaging chamber is sufficient to maintain adequate hydrostatic head for the circulation pump to prevent cavitation and maintain forced circulation of the saltwater.

3.4. Commercial system projection

A number of changes to the pilot configuration will be made for the commercial process system design in order to increase flexibility, which in turn will increase the PR value over a wide range of operating conditions. Furthermore, a commercial implementation should implement

more heat exchangers for better heat integration in order to maximize first- and second-law efficiencies.

The most effective way to increase the PR value and decrease the SC value is to increase the number of distillation effects in the MED system. Ideally, an AHP should be operated with no more than around 30 °C temperature lift in order to minimize entropic losses. Considering a temperature difference between the MED effects of about $\Delta T = 3$ °C, this means that the commercial system should have about 10 effects. In [25,34] a 14-effect MED system was employed. Although exhibiting higher PR and lower SC values than a 10-effect MED, a 14-effect MED leaves very little margin for any performance degradation caused by scaling on the heat transfer surfaces of the MED. However, the 14-effect MED of [25,34] has integrated heat exchangers for reducing the temperature of the condensate by preheating the feed. In order to maximize the efficiency of the process, a commercial system must incorporate similar heat exchangers to capture the heat of the product water before it is lost to the environment.

The integration of the AHP to the MED will be the same as in the pilot system in that the steam produced in the generator will be the condensing steam driving evaporation in the first effect. However, a secondary source of steam will be added to this stream. The secondary source of steam will be produced from the absorber heat as an alternative cooling configuration to the pilot which preheats the saltwater feed with this heat. After the steam condenses in the first effect, a fraction is looped back to the absorber as cooling water similar to the closed-loop boiler configuration during the MED-only operations. By decoupling the saltwater feed rate from the heat pump, the combined cycle will be more flexible and allow for the operation at high recovery without negatively impacting performance. Furthermore, depending on the application, an open-cycle double-effect AHP may be favored (e.g. an open-cycle version of the double-effect AHP of [25,34]). Such devices have been known to have a higher second-law efficiency and therefore can have a COP for heating of up to 2.3. Furthermore, the open-cycle implementation will reduce capital cost and be more efficient from both a first- and second-law perspective when integrated with the MED system.

An open-cycle double-effect AHP using the LiBr–H_2O pair was modeled as coupled to a 10-effect MED with intermediate feed preheating such as in [25,34]. The simulation results show a PR value of 18.4 and an SC value of 34.9 kWh_{th}/m^3. With the implementation of 10 effects and the feed preheat heat exchangers, all streams leaving the system are no more than 39 °C. In the summer time, this is very close to ambient and no more than about 12 °C above the available cooling water source, minimizing entropic losses.

4. Conclusion

A first-of-its-kind solar-powered desalination process system was demonstrated for high recovery of high scaling propensity agricultural drainage water as a water reuse strategy at the Panoche Water & Drainage District in California's Central Valley. The system was designed with the energy–water nexus in mind in order to decouple water production from energy production as well as limit the use of fossil fuels by turning to renewables in the form of solar-thermal power.

The system was operated both with and without the AHP in order to demonstrate its effectiveness at reducing the overall energy requirement of the process. The experimental and simulation results showed fairly good agreement. The AHP–MED system performed very favorably from both an energy consumption viewpoint as well as a robustness viewpoint. The final results are summarized below.

- MED-only operated at a maximum PR of 2.522 and a minimum SC of 261.87 kWh_{th}/m^3.
- AHP–MED operated at a maximum PR of 5.269 and a minimum SC of 133.2 kWh_{th}/m^3.
- Design and simulation of an optimal AHP–MED utilizing ten distillation effects showed a PR of 18.4 and an SC of 34.9 kWh_{th}/m^3.
- Measured degradation of the first distillation effect overall heat transfer coefficient attributed to scaling which was recoverable with short-downtime non-toxic in-situ cleaning.
- No degradation in overall system performance (from a first-law perspective) was measured as a result of scaling.

The future research objectives with this project will include performing a rigorous analysis of the thermodynamics of the fully-combined solar-AHP–MED process system. This will allow for further optimization of the system as currently configured by identifying the largest source(s) of irreversibilities in the current implementation. Furthermore, two new devices will be incorporated into the pilot system: thermal storage for off-peak operation and an integrated brine crystallizer for zero-liquid discharge. Finally, upon completion of these tasks and utilizing the results obtained with this study, a larger-scale solar-AHP–MED will be constructed at the same site as a long-term agricultural drainage reuse solution.

Acknowledgments

The authors would like to acknowledge the generous support from the State of California Department of Water Resources and the Panoche Water and Panoche Drainage Districts for funding this research.

References

[1] S. Lattemann, Development of an Environmental Impact Assessment and Decision Support System for Seawater Desalination Plants(Ph.D. thesis) TU Delft, 2010.
[2] World Bank, Renewable energy desalination: an emerging solution to close the water gap in the Middle East and North Africa, Tech. rep. World Bank, 2012.
[3] WaterWorld, Global desalination capacity growing substantially, finds study, http://www.waterworld.com/articles/2013/10/global-desalination-capacity-tops-80-million-cubic-meters-per-day.htmlOct 2013 (Accessed: May 2014).
[4] N. Ghaffour, T.M. Missimer, G.L. Amy, Technical review and evaluation of the economics of water desalination: current and future challenges for better water supply sustainability, Desalination 309 (2013) 197–207.
[5] K. Hussey, N. Carter, W. Reinhardt, Energy sector transformation: implications for water governance, Aust. J. Water Resour. 17 (2) (2013) 170–179, http://dx.doi.org/10.7158/W13-025.2013.17.2.
[6] WWAP (United Nations World Water Assessment Programme, The United Nations World Water Development Report 2014: Water and Energy, Tech. rep. UNESCO, Paris, 2014.
[7] California DWR, California agricultural water Use, http://www.water.ca.gov/wateruseefficiency/agricultural (Accessed: April 2014).
[8] M. Belkacem, S. Bekhti, K. Bensadok, Groundwater treatment by reverse osmosis, Desalination 206 (2007) 100–106, http://dx.doi.org/10.1016/j.desal.2006.02.062.
[9] R. Sobhani, M. Abahusayn, C.J. Gabelich, D. Rosso, Energy Footprint analysis of brackish groundwater desalination with zero liquid discharge in inland areas of the Arabian Peninsula, Desalination 291 (2012) 106–116, http://dx.doi.org/10.1016/j.desal.2012.01.029.
[10] B.C. McCool, A. Rahardianto, J. Faria, K. Kovac, D. Lara, Y. Cohen, Feasibility of reverse osmosis desalination of brackish agricultural drainage water in the San Joaquin Valley, Desalination 261 (2010) 240–250, http://dx.doi.org/10.1016/j.desal.2010.05.031.
[11] J. Thompson, A. Rahardianto, H. Gu, M. Uchymiak, A. Bartman, M. Hedrick, D. Lara, J. Cooper, J. Faria, P.D. Christofides, Y. Cohen, Rapid field assessment of RO desalination of brackish agricultural drainage water, Water Res. 47 (8) (2013) 2649–2660, http://dx.doi.org/10.1016/j.watres.2013.02.013.
[12] M. Elimelech, W.A. Phillip, The future of seawater desalination: energy, technology, and the environment, Science 333 (August) (2011) 712–717.
[13] D. Cohen-Tanugi, R.K. McGovern, S.H. Dave, J.H. Lienhard, J.C. Grossman, Quantifying the potential of ultra-permeable membranes for water desalination, Energy Environ. Sci. 7 (3) (2014) 1134–1141, http://dx.doi.org/10.1039/c3ee43221a.
[14] H. El-Dessouky, H. Ettouney, H. Al-Fulaij, F. Mandani, Multistage flash desalination combined with thermal vapor compression, Chem. Eng. Process. 39 (4) (2000) 343–356.
[15] H. Ettouney, Conventional thermal processes, in: G. Micale, L. Rizzuti, A. Cipollina (Eds.), Seawater Desalination, Green Energy and TechnologySpringer, Berlin Heidelberg, 2009, pp. 17–40, http://dx.doi.org/10.1007/978-3-642-01150-4 (Ch. 2).
[16] O. Morin, Design and operating comparison of MSF and MED systems, Desalination 93 (1993) 69–109, http://dx.doi.org/10.1016/0011-9164(93)80097-7.
[17] F. Al-Juwayhel, H. El-Dessouky, H. Ettouney, Analysis of single-effect evaporator desalination systems combined with vapor compression heat pumps, Desalination 114 (1997) 253–275, http://dx.doi.org/10.1016/S0011-9164(98)00017-4.
[18] H. El-Dessouky, I. Alatiqi, S. Bingulac, H. Ettouney, Steady-state analysis of the multiple effect evaporation desalination process, Chem. Eng. Technol. 21 (5) (1998) 437–451, http://dx.doi.org/10.1002/(SICI)1521-4125(199805)21:5<437::AID-CEAT437>3.0.CO;2-D.

[19] A.S. Nafey, H.E.S. Fath, A.A. Mabrouk, Thermo-economic investigation of multi effect evaporation (MEE) and hybrid multi effect evaporation–multi stage flash (MEE–MSF) systems, Desalination 201 (2006) 241–254, http://dx.doi.org/10.1016/j.desal.2005.09.044.
[20] T.H. Dahdah, A. Mitsos, Structural optimization of seawater desalination: I. A flexible superstructure and novel MED–MSF configurations, Desalination 344 (2014) 252–265, http://dx.doi.org/10.1016/j.desal.2014.03.030.
[21] K.H. Mistry, R.K. McGovern, G.P. Thiel, E.K. Summers, S.M. Zubair, J.H. Lienhard V, Entropy generation analysis of desalination technologies, Entropy 13 (12) (2011) 1829–1864, http://dx.doi.org/10.3390/e13101829.
[22] World Bank, Renewable Energy Desalination: An Emerging Solution to Close the Water Gap in the Middle East and North Africa, International Bank for Reconstruction and Development, Washington, D.C., 2012
[23] T.H. Dahdah, A. Mitsos, Structural optimization of seawater desalination: II Novel MED–MSF–TVC configurations, Desalination 344 (2014) 219–227, http://dx.doi.org/10.1016/j.desal.2014.03.026.
[24] A. Ophir, F. Lokiec, Advanced MED process for most economical sea water desalination, Desalination 182 (2005) 187–198, http://dx.doi.org/10.1016/j.desal.2005.02.026.
[25] D.C. Alarcón-Padilla, L. García-Rodríguez, J. Blanco-Gálvez, Assessment of an absorption heat pump coupled to a multi-effect distillation unit within AQUASOL project, Desalination 212 (2007) 303–310, http://dx.doi.org/10.1016/j.desal.2006.10.015.
[26] B.B. Saha, K.C. Ng (Eds.), Advances in Adsorption Technology, Nova Science Publishers, Inc., New York, 2010.
[27] K.E. Herold, R. Radermacher, S.A. Klein, Absorption Chillers and Heat Pumps, CRC Press, New York, 1996.
[28] D. Zejli, R. Benchrifa, A. Bennouna, O. Bouhelal, A solar adsorption desalination device: first simulation results, Desalination 168 (2004) 127–135, http://dx.doi.org/10.1016/j.desal.2004.06.178.
[29] X. Wang, K.C. Ng, Experimental investigation of an adsorption desalination plant using low-temperature waste heat, Appl. Therm. Eng. 25 (17–18) (2005) 2780–2789, http://dx.doi.org/10.1016/j.applthermaleng.2005.02.011.
[30] X. Wang, K.C. Ng, A. Chakarborty, B.B. Saha, How heat and mass recovery strategies impact the performance of adsorption desalination plant: theory and experiments, Heat Transf. Eng. 28 (2) (2007) 147–153, http://dx.doi.org/10.1080/01457630601023625.
[31] K.C. Ng, K. Thu, Y. Kim, A. Chakraborty, G. Amy, Adsorption desalination: an emerging low-cost thermal desalination method, Desalination 308 (2013) 161–179, http://dx.doi.org/10.1016/j.desal.2012.07.030.
[32] S. Aly, Vapour compression distillation using waste heat absorption systems, Desalination 68 (1) (1988) 57–68, http://dx.doi.org/10.1016/0011-9164(88)80042-0.
[33] K. Fathalah, S.E. Aly, Theoretical study of a solar powered absorption/MED combined system, Energy Convers. Manag. 31 (6) (1991) 529–544.
[34] D.C. Alarcón-Padilla, L. García-Rodríguez, J. Blanco-Gálvez, Experimental assessment of connection of an absorption heat pump to a multi-effect distillation unit, Desalination 250 (2) (2010) 500–505, http://dx.doi.org/10.1016/j.desal.2009.06.056.
[35] F. Mandani, H. Ettouney, H. El-Dessouky, LiBr–H_20 absorption heat pump for single-effect evaporation desalination process, Desalination 128 (2000) 161–176.
[36] Open Source Modelica Consortium, OpenModelica user's guide, OpenModelica Version 1.9.1, 2013.
[37] M.H. Sharqawy, J.H. Lienhard V, S.M. Zubair, Thermophysical properties of seawater: a review of existing correlations and data, Desalin. Water Treat. 16 (2010) 354–380, http://dx.doi.org/10.5004/dwt.2010.1079.
[38] W.F. Davidson, D.C. Erickson, 260 °C aqueous absorption working pair under development, IEA Heat Pump Cent. Newsl. 4 (3) (1986) 29–31.
[39] W.F. Davidson, D.C. Erickson, New high temperature absorbent for absorption heat pumps, Final Report, Energy Concepts, 1986.
[40] M.R. Ally, Thermodynamic properties of aqueous ternary solution relevant to chemical heat pumps, Final Report ORNL/TM-10258, Oak Ridge National Laboratory, 1987.
[41] M. Bourouis, M.E. Alvarez, X. Esteve, Vapor–liquid equilibrium of aqueous alkaline nitrate and nitrite solutions for absorption refrigeration cycles with high-temperature driving heat, J. Chem. Eng. Data 56 (2011) 491–496, http://dx.doi.org/10.1021/je1008894.